ACS APPLIED MATERIALS & INTERFACES

Research Article

www.acsami.org

Aligned Magnetic Domains in *p*- and *n*-Type Ferromagnetic Nanocrystals and in *pn*-Junction Nanodiodes

Abhijit Bera and Amlan J. Pal*

Department of Solid State Physics, Indian Association for the Cultivation of Science, Jadavpur, Kolkata 700032, India

Supporting Information

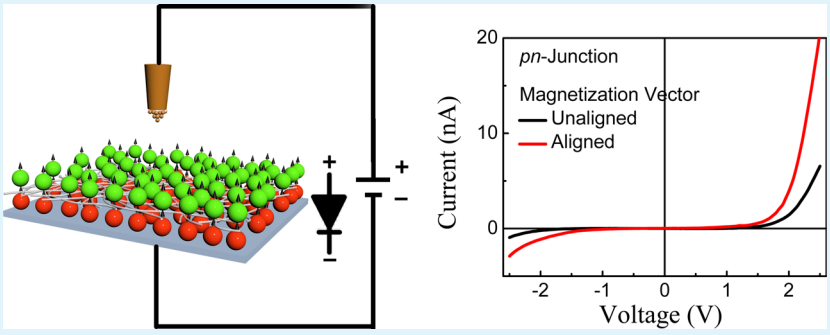

ABSTRACT: We form *pn*- and *np*-junctions between monolayers of *p*- and *n*-type nanocrystals that exhibit current rectification in the nanodiodes when characterized with a scanning tunneling microscope (STM) tip. With the use of ferromagnetic nanocrystals, we study the effect of mutual alignment of magnetization vectors on current rectification in the junction between the two nanocrystals. We show that when the magnetization vectors of the *p*- and of the *n*-type nanocrystals are parallel to each other (and both facing toward the apex of the STM tip) tunneling current in both bias modes increases with correspondingly a higher rectification ratio. This is in contrast to the parameters of the nanodiodes in which magnetization vectors of the components are unaligned or randomized. To analyze the results, we record scanning tunneling spectroscopy of the monolayer of the components having magnetization vectors aligned or unaligned to locate their valence and conduction band edges and to determine the effect of the alignment on the band edges. Upon alignment of the magnetization vectors of the nanocrystals in a monolayer, the conduction band edge of the *p*-type and valence band edge of the *n*-type semiconductor shift towards the Fermi energy leading to a change in energy levels of the *pn*-junctions and accounting for the improved parameters of the nanodiodes.

KEYWORDS: *junction between ferromagnetic nanocrystals, nanodiodes, current rectification, effect of alignment of magnetization vectors on rectification, scanning tunneling spectroscopy*

1. INTRODUCTION

Since *pn*-junction diodes are one of the most fundamental components of electronics, use of lower-dimensional materials as current rectifiers is of immense interest among researchers. Nanostructures considered in this direction are two-dimensional graphenes,[1,2] one-dimensional nanowires,[3−5] and finally zero-dimensional quantum dots.[6,7] A wide variety of materials including ZnO have been used to fabricate such lower-dimensional junction diodes.[1−8] The use of ZnO nanocrystals in forming nanodiodes evolved primarily due to their facile growth procedure and also due to the possibility to introduce dopants during the growth of colloidal quantum dots (CQDs).

Use of doped ZnO is generally of interest in inducing *n*- or *p*-type conduction processes. Another dimension is added to the research on ZnO nanostructures when they are doped with 3d transition elements, such as Mn, Co, and Ni, introducing dilute magnetic semiconducting (DMS) properties, the appearance of which largely depends on the growth process.[9−12] In this class of semiconductors, magnetic ions present in the nanocrystals lead to an exchange interaction between the s−p band electrons and the spin-localized d-state electrons at the magnetic ions, resulting in interesting magnetic properties.[13,14] In a series of articles, Gamelin and his co-workers have reported and explained hole-mediated ferromagnetism in Mn-doped ZnO through an incorporation of uncompensated *p*-type defects.[13−15] Similarly, in Co-doped ZnO, the electron-mediated ferromagnetism has been shown to occur through uncompensated *n*-type defects.[9,14] In both the cases, the nature of capping to passivate the surface defects played a major role in determining the nature of the conduction process.[13]

Thin films of ferromagnetic semiconductors have been used to form light-emitting diodes[16] or various junctions[17−19] to study the magnetic field dependence of forward-bias current. Use of ferromagnetic nanocrystals as lower-dimensional materials in *pn*-junction rectifiers would be innovative since the mutual alignment of the magnetization vector of the two

Received: September 10, 2013
Accepted: October 28, 2013
Published: October 28, 2013

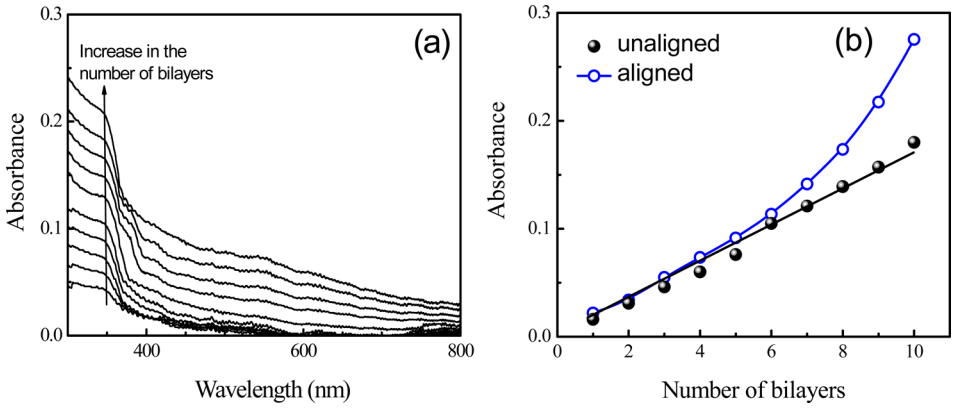

Figure 1. (a) Optical absorption of PAH/Co@ZnO/PAH/Mn@ZnO LbL films recorded after adsorption of each bilayer. (b) A plot of adsorption at 350 nm versus number of bilayers for films deposited (i) without any magnetic field, i.e., a conventional LbL film, and (ii) with the assistance of a magnetic field. In the latter case that can be termed as "magnetic moment assisted" assembly, a magnetic field of 330 mT was applied to the film before adsorption of the next monolayer.

components may dictate the parameters of the junction diode. In this work, we present the effect of aligned magnetic domains in *p*- and *n*-type ferromagnetic nanocrystals and in *pn*-junction nanodiodes.

2. EXPERIMENTAL SECTION

Growth of Nanocrystals. ZnO nanocrystals were grown following a colloidal synthesis route through a reaction of an ethanol solution of tetramethylammonium hydroxide (TMAH), $N(CH_3)_4OH{\cdot}5H_2O$, and zinc acetate dihydrate, $Zn(O_2CCH_3)_2{\cdot}(H_2O)_2$, which was dissolved in dimethyl sulfoxide (DMSO). In a typical reaction that was carried out in a three-neck flask at room temperature, 20 mL of TMAH solution (0.552 M) in ethanol was added dropwise (2 mL/min) to 60 mL of zinc acetate dihydrate (0.101 M) under a constant stirring condition. The reaction mixture turned turbid indicating formation of ZnO nanocrystals. The reaction was terminated by adding copious ethyl acetate, and the solution was centrifuged to separate the nanocrystals and washed in DMSO in an iterative manner.

Co^{2+} doping in ZnO nanocrystals was achieved by the addition of a measured amount of cobalt(II) acetate tetrahydrate, $Co(O_2CCH_3)_2{\cdot}(H_2O)_4$, in the precursor solution so that a predetermined [Co]:[Zn] concentration ratio is achieved.[9] In the present work, we controlled the content of Co^{2+} in Zn^{2+} ions in the reaction flask to be 2 atomic %.

Doping with Mn^{2+} ions was similarly introduced by an addition of manganese(II) acetate tetrahydrate, $Mn(O_2CCH_3)_2{\cdot}(H_2O)_4$, in the precursor solution.[10] Here also, we aimed to achieve 2 atomic % of manganese in the ZnO nanocrystals.

Since we would be forming a monolayer of the doped nanocrystals through a layer-by-layer electrostatic-assembly (LbL) approach, we introduced trioctylphosphine oxide (TOPO) and trioctylamine as capping agents for Co-doped and Mn-doped ZnO nanocrystals, respectively. To do so, the as-grown nanocrystals were stirred in TOPO (and trioctylamine) environment at 180 °C for 30 min. While TOPO introduces solubility of Co-doped ZnO nanocrystals in toluene, boiling of Mn-doped ZnO in trioctylamine under nitrogen environment is known to improve the ferromagnetic nature of the nanocrystals.[15] The nanocrystals were separated from the reaction flask and redispered in toluene for characterization and formation of LbL assembly.

Characterization of the Nanocrystals. The doped nanocrystals were characterized by optical absorption spectroscopy, X-ray diffraction (XRD), energy-dispersive X-ray (EDX) spectroscopy, transmission electron microscopy (TEM), and high-resolution TEM (HR-TEM). Details of the results and the analysis can be found in Figures S1 and S2 in the Supporting Information.

Formation of Monolayers and *pn*-Junctions through the Layer-by-Layer (LbL) Assembly Process. Formation of a monolayer of the nanocrystals and a heterojunction between two monolayers was a part of the LbL film-deposition procedure which relies on an electrostatic assembly process followed by van der Waals force.[20,21] Here, after the adsorption is initiated by amines, van der Waals attraction took over for subsequent adsorption. They were formed on highly doped Si⟨111⟩ substrates having a resistivity of 3−10 mΩ.cm. The substrates were deprotonated by overnight treatment in H_2O_2:NH_4OH (1:3) solution. Apart from forming a monolayer of Co- and Mn-doped ZnO nanocrystals separately, heterojunctions were formed between monolayers of the two types of nanocrystals. Two types of junctions were formed: (1) a junction between a monolayer of Co-doped and a monolayer of Mn-doped ZnO nanocrystals in sequence that could be termed as an *np*-junction and (2) a junction in reverse sequence, that is Mn@ZnO/Co@ZnO, that can be termed as a *pn*-junction. Characterization of *np*- and *pn*-junctions with the same set of electrodes enabled us to separate out the junction characteristics from the effect of the interfaces with the electrodes.

In practice, a monolayer of Co-doped (or Mn-doped) ZnO nanocrystals was formed by dipping the Si-electrode in aqueous solution of PAH and toluene solution of the nanocrystals in sequence. During the dipping in a solution of nanocrystals, a mild stirring was used to avoid precipitation and for improved adsorption. Each dipping was followed by three washings in appropriate solvents to remove unbound moieties from the surface. To form multilayers of the nanocrystals for optical characterization, the dipping sequence was cycled for a desired number of time. To form the *np*- and *pn*-junctions, monolayers of the nanocrystals were adsorbed in the desired sequence. That is, to form a *pn*-junction on a Si substrate, monolayers were formed in the following order: Si/PAH/Mn@ZnO/PAH/Co@ZnO.

Characterization of Monolayers and *pn*-Junctions. Monolayers of the Co-doped and Mn-doped ZnO nanocrystals and the junctions between the two monolayers were characterized with a scanning tunneling microscope (STM) (NanoSurf easyScan2) in an ambient condition. The Pt/Ir tip was used as the top electrode to apply voltage and to measure the tunneling current. Bias was applied with respect to the Si electrode.

Since we have used ferromagnetic nanocrystals in the present work, we used two types of substrate holders, namely, a nonmagnetic and a magnetic holder, for STM characterization. The field of the latter substrate (100 mT) was enough to retain the alignment of the magnetization vectors of the nanocrystals in a monolayer. (While forming a multilayer of Co-doped ZnO nanocrystals, if a magnetic field was applied after formation of each monolayer, the LbL film deposition process was found to be augmented due to the magnetic force of attraction of aligned ferromagnetic nanocrystals on the monolayer supplementing the adsorption process of the subsequent layers.[22] The field required to achieve such an augmentation in the LbL assembly process, as evidenced by an enhancement in the optical absorption spectrum, was 200 mT. Such a field can be termed as the saturation field for the Co-doped ZnO nanocrystals. The value

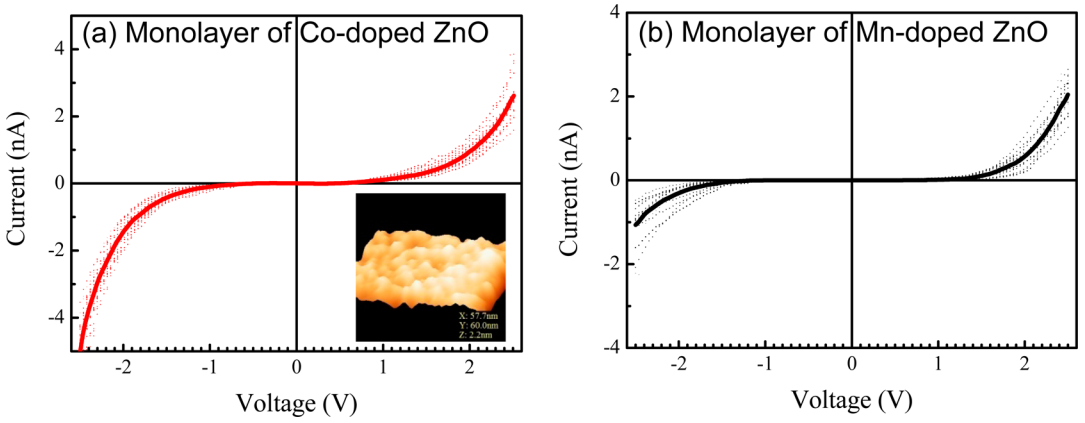

Figure 2. Current–voltage characteristics of a monolayer of (a) Co- and (b) Mn-doped ZnO nanocrystals. In each of the plots, results obtained from 20 different points on a monolayer are shown as dotted lines with the thick line being the average of the 20 characteristics. STM topography of a monolayer of Co-doped ZnO nanocrystals is shown in the inset of (a).

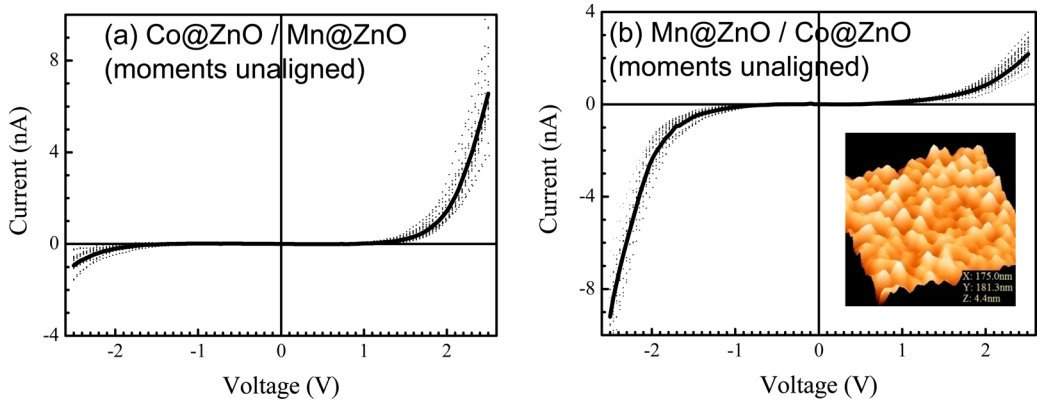

Figure 3. Current–voltage characteristics of (a) Co@ZnO/Mn@ZnO and (b) Mn@ZnO/Co@ZnO junctions recorded at 20 different points each. Here, the junctions were formed between monolayers of the two nanocrystals. The thick lines in each of the two plots are the average of the characteristics. STM topography of a Mn@ZnO/Co@ZnO junction is shown in the inset.

matches well with the saturation field of magnetization versus magnetic field strength loop plot[9]). For Mn-doped ZnO nanocrystals, the saturation field was 150 mT.[10] To ensure alignment of the magnetization vectors, the monolayers and the junctions were placed in a 330 mT field before mounting on the magnetic substrate holder. Such a substrate holder retained the alignment of magnetization vectors of the nanocrystals and enabled us to characterize the monolayers and the junctions with the magnetization vectors aligned perpendicular to the substrate and facing upwards. We compared such characteristics with that when their magnetization vectors were unaligned or randomized.

3. RESULTS AND DISCUSSION

Junction Formation. As stated in the Experimental Section, junctions were formed between a monolayer of Co-doped ZnO nanocrystals (*n*-type) and a monolayer of Mn-doped ones (*p*-type). Since monolayer formation was a part of the LbL film deposition process, it is imperative to show how the film formed layer after layer. In Figure 1a, we show optical absorption of the film for a different number of PAH/Co@ZnO/PAH/Mn@ZnO bilayers. While the absorption profile of the LbL films matched that of the nanocrystals in dispersed solution, the absorbance of the film grew linearly with the number of bilayers (Figure 1b).

In support of the thesis that magnetization vectors of the nanocrystals could be aligned in each monolayer, we formed multilayered films of such aligned nanocrystals. Since we aligned the magnetization vector perpendicular to the substrate and facing outwards, the magnetic force of attraction augmented the adsorption process of the subsequent layers; that is, the (magnetically) aligned nanocrystals supplemented formation of further layers. The absorbance of such aligned films grew at a faster rate (Figure 1b). This meant that magnetic moments of nanocrystals in the previously deposited layers participated in augmenting the adsorption process. Apart from the usual force of attraction active in the LbL assembly process, the magnetic force due to the aligned magnetization of ferromagnetic nanocrystals on the substrate is the driving force for the "magnetic moment assisted" LbL adsorption process.

***I–V* of the *pn*-Junctions and the Components.** We have characterized the monolayer of Co@ZnO and Mn@ZnO nanocrystals with a STM tip. A typical topography of a Co@ZnO monolayer is presented in the inset of Figure 2(a) that evidences the presence of the nanocrystals on the silicon substrate. Tunneling current versus voltage characteristics were recorded at many different points on the monolayer. Tip approaching current was kept low so that the tip did not influence the energy states of the nanocrystals. Results from 20 points on the monolayer of Co@ZnO and Mn@ZnO along with the average of the respective characteristics are shown in Figures 2(a) and 2(b), respectively. For both the nanocrystals, the *I–V* plots were largely symmetric. A little asymmetry may

dx.doi.org/10.1021/am4039147 | ACS Appl. Mater. Interfaces 2013, 5, 12083–12088

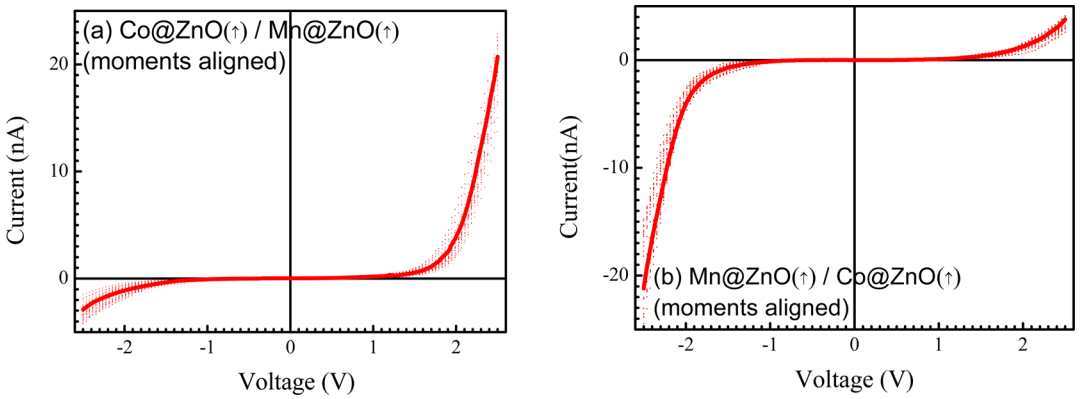

Figure 4. Current–voltage characteristics of (a) Co@ZnO(↑)/Mn@ZnO(↑) and (b) Mn@ZnO(↑)/Co@ZnO(↑) junctions recorded at 20 different points each. Here, the junctions, formed between monolayers of the two nanocrystals, have their components' moments parallel to each other (aligned perpendicular to the substrate and facing upwards). The thick lines in each of the two plots are an average of the characteristics.

have arisen due to the difference in the work function of the two electrodes.

We have characterized the heterojunction between the two monolayers. We have considered both possibilities, that is, Co@ZnO/Mn@ZnO and Mn@ZnO/Co@ZnO on silicon electrode substrates, which may be termed as an *np*- and a *pn*-junction, respectively. Tunneling current versus tip voltage characteristics of the two junctions, recorded at many different points along with the averages, are shown in Figures 3(a) and 3(b), respectively. Both the plots show rectifying characteristics. Since the voltage was applied with respect to the silicon electrode substrate, the Co@ZnO/Mn@ZnO (*np*-junction) was forward biased at a positive tip voltage. Similarly, the usual *pn*-junction (Mn@ZnO/Co@ZnO) was reverse biased at a positive tip voltage. The rectifying characteristics of the junctions, as presented in Figures 3(a) and 3(b), hence comply with the nature of diode junctions. More importantly, since the direction of rectification is opposite to each other in Co@ZnO/Mn@ZnO and Mn@ZnO/Co@ZnO junctions while keeping the electrode combinations the same, we could rule out the effect of interfaces and infer that the junctions between the two monolayers were indeed rectifying in nature. The results hence evidence formation of nanodiodes.

Effect of Alignment of Magnetization Vectors on the *I*–*V*'s. In this work, we used ferromagnetic nanocrystals in forming a junction between the two types of semiconductors that can be termed as a nanodiode to study the effect of alignment of magnetization vectors on the rectification. Since we could align the vectors parallel to each other and both of them perpendicular to the substrate pointing outwards, we characterized such an aligned junction. The *I*–*V* characteristics of the two aligned junctions, that can be denoted as Co@ZnO(↑)/Mn@ZnO(↑) and Mn@ZnO(↑)/Co@ZnO(↑), are shown in Figures 4(a) and 4(b), respectively. It may be pointed out here that we could not form a junction with magnetization vectors antiparallel to each other, for example, Co@ZnO(↑)/Mn@ZnO(↓) or some other combination, since the saturation field of the two ferromagnetic nanocrystals is similar and an opposing field applied to the second monolayer would have realigned the domains of the nanocrystals in the first layer.

Figure 4 shows that the aligned junctions, Co@ZnO(↑)/Mn@ZnO(↑) and Mn@ZnO(↑)/Co@ZnO(↑), also acted as rectifiers. In the aligned junctions too, the direction of rectification in *np*- and *pn*-systems is opposite to each other. If we compare the results of the unaligned and aligned rectifiers (Table 1), we find that upon alignment the magnitude of current under both the biases increased with a further increase

Table 1. Magnitude of Current under a Forward and a Reverse Bias along with the Rectification Ratio of Different *pn*- and *np*-Junctions

	magnitude of current under 2.5 V		
junction	forward bias (nA)	reverse bias (nA)	rectification ratio
np	6.6	1.2	5.5
n(↑)*p*(↑)	19.5	2.8	7.0
pn	9.4	2.1	4.5
p(↑)*n*(↑)	21.5	3.3	6.5

in the rectification ratio. It may be pointed out that the large area *pn*- and *np*-junctions based on multilayered films of the *p*- and of the *n*-type nanocrystals sandwiched between a base electrode and a thermally evaporated metal electrode showed rectifying *I*–*V* characteristics along with the rectification responding (increasing) when the domains of the ferromagnetic nanocrystals were aligned parallel to each other. In the following, we will explain the rationale behind such an observation in the nanodiodes by considering the energy of the conduction and valence band edges (CB and VB, respectively).

Aligned Magnetic Domains: Effect on Band Edges of the Junction. To analyze the observation that the junctions between the two types of nanocrystals with aligned magnetization vectors return a higher rectification ratio, it is imperative to locate the band edges of the nanocrystals in a monolayer before and after alignment of the magnetization vectors. To do so, we have plotted the *I*–*V* characteristics of the two monolayers in a log-linear scale. The characteristics of Co- and Mn-doped ZnO nanocrystals, as shown in Figures 5(a) and 5(b), respectively, show an increase in current at two voltages. With STM measurements, the voltages at which the amplitude of current starts to increase from its background level signify energies at which the tip metal's work function matches the conduction and the valence band edge of the nanocrystals on the base electrode.[23,24] While at the positive voltage offset (with respect to the tip metal's work function), electrons can be withdrawn from the nanocrystals to the tip denoting the location of the valence band edge, and the negative voltage offset would allow injection of electrons from the tip providing the location of the conduction band edge of the nanocrystals.

dx.doi.org/10.1021/am4039147 | *ACS Appl. Mater. Interfaces* 2013, 5, 12083–12088

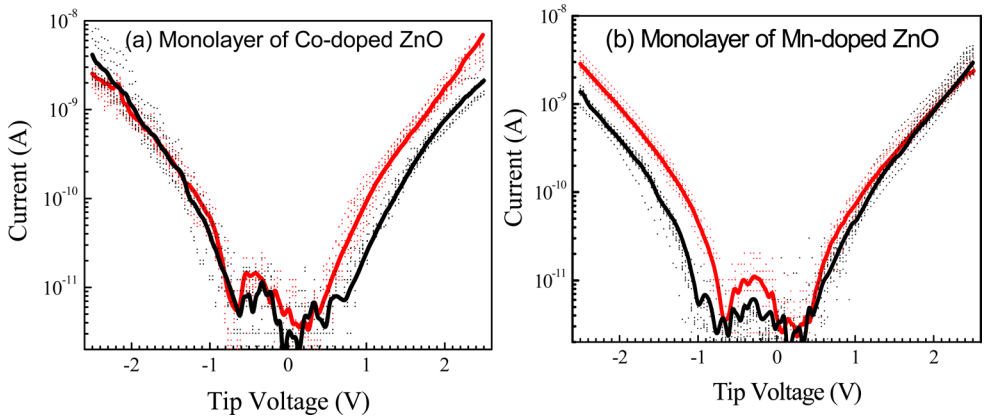

Figure 5. Current−voltage characteristics in a log-linear scale. A monolayer of (a) Co- and (b) Mn-doped ZnO nanocrystals was characterized with their magnetization vectors unaligned (black lines) and aligned (red lines) perpendicular to the substrate and facing upwards and parallel to each other. The thick lines in each of the plots are an average of the 20 characteristics in each configuration.

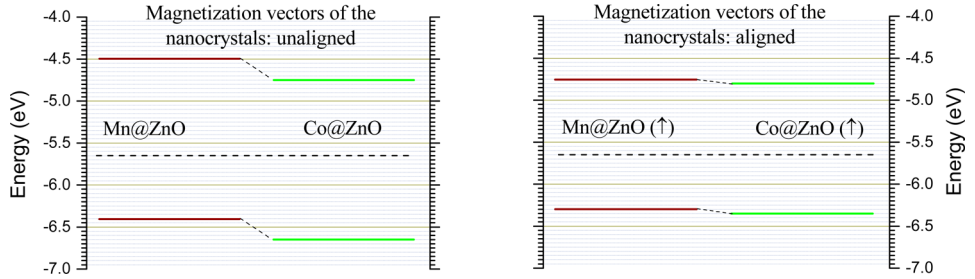

Figure 6. Energy levels of Mn@ZnO/Co@ZnO and Mn@ZnO(↑)/Co@ZnO(↑) *pn*-junctions.

The 0 V in the plots denotes the work function of the tip that is matched with the Fermi energy of the semiconductors. The results hence primarily confirmed the *n*- and *p*-type nature of Co-doped and Mn-doped ZnO nanocrystals, respectively.

In each of the plots of Co- and Mn-doped ZnO nanocrystals, we have added characteristics of unaligned and aligned monolayers. The alignment was perpendicular to the substrate with magnetization vectors pointing upwards (away from the substrate). The results show that upon alignment of the magnetization vectors one of the voltages at which the amplitude of current increases from the background level changes. The shift in the voltage in both the cases is towards the 0 V. This implies that one of the band edges shifts towards the Fermi energy. The change in the other band edge is low or minimal. While the conduction band edge changes in the *p*-type nanocrystals upon alignment, the *n*-type one manifests an increase in the valence band edge due to the ordering of the vectors. That is, the band that is away from the Fermi energy was more affected due to the alignment. We earlier studied the role of magnetization vectors on the transport gap of ferromagnetic nanocrystals.[22] We have explained that the aligned magnetic domains may have interacted with each other to lower the transport gap of the nanocrystals.

With a change in one of the band edges due to an alignment of magnetization vectors, it is interesting to look at the reorganized band structures of the *pn*-junction (Figure 6). In the figure, we have plotted the energy levels of Mn@ZnO/Co@ZnO and Mn@ZnO(↑)/Co@ZnO(↑) *pn*-junctions. It may be recalled that the Mn@ZnO(↑)/Co@ZnO(↑) signifies a junction where the magnetization vectors of the *p*- and *n*-type nanocrystals are aligned parallel (both facing upwards). Upon alignment that prompted in a decrease in the conduction band edge of the *p*-type and an increase in the valence band edge of the *n*-type nanocrystals, the offset between the conduction band edges and valence band edges (V_0) of the two materials decreased (Figure 6). Such a change in the band diagram of a junction led to an increase in the current of $p(\uparrow)n(\uparrow)$ and $n(\uparrow)p(\uparrow)$ nanodiodes under both the bias modes as compared to the conventional (unaligned) *pn*- and *np*-junctions, respectively (Table 1). The former junctions moreover returned a higher rectification ratio as compared to the respective unaligned junctions.

From the expression of diode equations, we could explain the results qualitatively. Due to a decrease in V_0 of a junction upon alignment of magnetization vectors, the forward bias current is expected to increase. Similarly, the (amplitude of) current in the reverse bias also increases due to the lowering of resistance that occurs as a result of narrowing of the width of the depletion region.

4. CONCLUSIONS

In summary, we have grown cobalt-doped ZnO (*n*-type) and manganese-doped ZnO (*p*-type) nanocrystals to form a junction between their monolayers on an electrode. The *pn*- and *np*-junctions when characterized with a scanning tunneling microscope tip evidenced rectification substantiating formation of nanodiodes. With the use of ferromagnetic nanocrystals, magnetization vectors of the nanocrystals of the nanodiodes could be aligned mutually parallel. Such (magnetically) aligned nanodiodes returned a higher current and also a higher rectification ratio. From the STS of the monolayers of the component nanocrystals, we have observed that upon alignment of magnetization vectors the band edge corresponding to the minority carriers of the semiconductors shifted towards the

Fermi energy. This led to reorganization of the energy levels of *pn-* (and *np-*) junctions explaining the change in the parameters of the nanodiodes.

■ ASSOCIATED CONTENT

Supporting Information

Detailed description of characterization of the nanocrystals along with optical absorption spectra and XRD patterns, TEM and HR-TEM images, and EDX analysis of Co- and Mn-doped ZnO nanocrystals (Figures S1 and S2). This material is available free of charge via the Internet at http://pubs.acs.org.

■ AUTHOR INFORMATION

Corresponding Author

*Tel.: +91-33-24734971. Fax: +91-33-24732805. E-mail: sspajp@iacs.res.in.

Notes

The authors declare no competing financial interest.

■ ACKNOWLEDGMENTS

AB acknowledges CSIR Fellowship No. 09/080(0779)/2011-EMR-I (Roll No. 510847). The authors acknowledge financial assistance from DST projects.

■ REFERENCES

(1) Yu, D. S.; Nagelli, E.; Naik, R.; Dai, L. M. *Angew. Chem., Int. Ed.* **2011**, *50*, 6575−6578.
(2) Kim, S.; Shin, D. H.; Kim, C. O.; Kang, S. S.; Kim, J. M.; Jang, C. W.; Loo, S. S.; Lee, J. S.; Kim, J. H.; Choi, S. H.; Hwang, E. *ACS Nano* **2013**, *7*, 5168−5174.
(3) Pradhan, B.; Batabyal, S. K.; Pal, A. J. *Appl. Phys. Lett.* **2006**, *89*, 233109.
(4) Sun, Y.; Fox, N. A.; Fuge, G. M.; Ashfold, M. N. R. *J. Phys. Chem. C* **2010**, *114*, 21338−21341.
(5) Li, G. H.; Sundararajan, A.; Mouti, A.; Chang, Y. J.; Lupini, A. R.; Pennycook, S. J.; Strachan, D. R.; Guiton, B. S. *Nanoscale* **2013**, *5*, 2259−2263.
(6) Mohanta, K.; Batabyal, S. K.; Pal, A. J. *Chem. Mater.* **2007**, *19*, 3662−3666.
(7) Radha, B.; Kulkarni, G. U. *Adv. Funct. Mater.* **2012**, *22*, 2837−2845.
(8) Khatei, J.; Rao, K. *AIP Adv.* **2011**, *1*, 042166.
(9) Schwartz, D. A.; Norberg, N. S.; Nguyen, Q. P.; Parker, J. M.; Gamelin, D. R. *J. Am. Chem. Soc.* **2003**, *125*, 13205−13218.
(10) Norberg, N. S.; Kittilstved, K. R.; Amonette, J. E.; Kukkadapu, R. K.; Schwartz, D. A.; Gamelin, D. R. *J. Am. Chem. Soc.* **2004**, *126*, 9387−9398.
(11) Garcia, M. A.; Ruiz-Gonzalez, M. L.; Quesada, A.; Costa-Kramer, J. L.; Fernandez, J. F.; Khatib, S. J.; Wennberg, A.; Caballero, A. C.; Martin-Gonzalez, M. S.; Villegas, M.; Briones, F.; Gonzalez-Calbet, J. M.; Hernando, A. *Phys. Rev. Lett.* **2005**, *94*, 217206.
(12) Sluiter, M. H. F.; Kawazoe, Y.; Sharma, P.; Inoue, A.; Raju, A. R.; Rout, C.; Waghmare, U. V. *Phys. Rev. Lett.* **2005**, *94*, 187204.
(13) Kittilstved, K. R.; Liu, W. K.; Gamelin, D. R. *Nat. Mater.* **2006**, *5*, 291−297.
(14) Kittilstved, K. R.; Norberg, N. S.; Gamelin, D. R. *Phys. Rev. Lett.* **2005**, *94*, 147209.
(15) Kittilstved, K. R.; Gamelin, D. R. *J. Am. Chem. Soc.* **2005**, *127*, 5292−5293.
(16) Chakrabarti, S.; Holub, M. A.; Bhattacharya, P.; Mishima, T. D.; Santos, M. B.; Johnson, M. B.; Blom, D. A. *Nano Lett.* **2005**, *5*, 209−212.
(17) Tulapurkar, A. A.; Suzuki, Y.; Fukushima, A.; Kubota, H.; Maehara, H.; Tsunekawa, K.; Djayaprawira, D. D.; Watanabe, N.; Yuasa, S. *Nature* **2005**, *438*, 339−342.
(18) Yamanaka, S.; Kanki, T.; Kawai, T.; Tanaka, H. *Nano Lett.* **2011**, *11*, 343−347.
(19) Joo, S.; Kim, T.; Shin, S. H.; Lim, J. Y.; Hong, J.; Song, J. D.; Chang, J.; Lee, H. W.; Rhie, K.; Han, S. H.; Shin, K. H.; Johnson, M. *Nature* **2013**, *494*, 72−76.
(20) Neves, M. C.; Pereira, A. S.; Peres, M.; Kholkin, A.; Monteiro, T.; Trindade, T. In *Advanced Materials Forum III, Pts 1 and 2*; Vilarinho, P. M., Ed.; Trans Tech Publications Ltd.: Zurich-Uetikon, 2006; Vol. *514-516*, pp 1111−1115.
(21) Sato, M.; Sano, M. *Langmuir* **2005**, *21*, 11490−11494.
(22) Chakrabarti, S.; Pal, A. J. *RSC Adv.* **2013**, *3*, 5022−5027.
(23) Walzer, K.; Quaade, U. J.; Ginger, D. S.; Greenham, N. C.; Stokbro, K. *J. Appl. Phys.* **2002**, *92*, 1434−1440.
(24) Ghosh, B.; Pal, A. J. *J. Phys. Chem. C* **2010**, *114*, 13583−13588.